Theoretical and Applied Mechanics Letters xxx (xxxx) xxx

Contents lists available at ScienceDirect

Theoretical and Applied Mechanics Letters

journal homepage: www.elsevier.com/locate/taml

Letter

On interaction between freely moving bodies and fluid in a channel flow

Qingsong Liu [a,*], Samire Yazar [b], Frank Smith [a]

[a] Department of Mathematics, UCL, Gower Street, London, WC1E 6BT, United Kingdom
[b] Department of Mathematics, Gebze Technical University, Gebze/Kocaeli, 41400, Turkey

ARTICLE INFO

Article history:
Received 19 September 2022
Revised 10 November 2022
Accepted 11 November 2022
Available online xxx

Keywords:
Particle movement
Channel flow
Impacts
Analysis
Computation

ABSTRACT

The interaction between free fast-moving bodies (or particles) and the fluid surrounding them is studied, motivated by applications in different branches of industry, biomedicine, the environment and science such as flying droplets, ice growth, dust, impacts, food grains, sport, complexity and storms. New inviscid-based modelling and results on the behaviour of two interacting bodies inside a channel flow are described. This is followed by discussion of the more-bodies extension with a view to treating arrays of bodies in a rational manner. Significant dependences on initial conditions and on the comparative body masses and moments of inertia are found for the occurrence of body-body impacts as opposed to wall-body impacts and for the associated impact times.

The motivation for this study on dynamic fluid/body interactions comes partly from the many practical application areas of these interactions. Included are significant issues of air vehicle safety concerned with the icing of external surfaces (wing, fuselage) or internal surfaces (engine) when impacted upon by ice particles, super-cooled liquid droplets or other bodies or particles [1–3]. Similar issues arise for land and sea transport. Another wide area is in biomedical science where relatively small particles such as treatment drugs or thrombi travel through blood vessels [4–6] which are often relatively long. Yet another area is centred on environmental applications, for example the movement of dirt, dust and sand, both on Earth and on other planets. Finally here the application to food-sorting can be mentioned, involving for example rice grains travelling down a chute in order to be investigated systematically for defects [7]. The motivation is also partly from the intrinsic scientific interest and challenge of the interactive area, as distinct from that of the classical problem of fluid flow around a fixed body. During a dynamic fluid/body interaction the fluid motion affects the body motion because of the induced flow forces acting on the body surface but the moving body in turn alters the fluid motion around it by virtue of (e.g.) the kinematic conditions on the body surface and so there is two-way coupling.

One of our prime aims is to increase physical understanding of the mechanisms involved. We use rational modelling based on reduced equations, which then tend to shed light on the mechanisms by means of analysis and reduced computation [7–12]. The study is meant to be complementary to direct numerical simulations [13–15]. In addition there has been much work on fluid/body interaction for a single body or particle: see inviscid-based theory in Refs. [7–12] and viscous-inviscid interaction theory in Ref. [16–19]. Among these works are found close connections between reduced-equation results of the type discussed in the current paper and the numerical findings from direct numerical simulation: see Refs. [16] and [19].

The specific interest in the present investigation is in fluid/body interactions for two or more bodies (finite-sized particles, objects) free to move in fluid within a straight-walled channel. This has practical connections with applications to engine dynamics [20] and food-sorting processes [21] in particular. Concerning the latter and its modelling, the situation is that many food objects such as peas or rice grains are projected down an inclined open chute for subsequent sorting [22]. The study in Ref. [7] addressed this scenario by consideration of many slender particles being present inside a channel through which fluid (air in their case) is flowing towards, around and past the particles in a coordinate

* Corresponding author.
E-mail addresses: ucahiux@ucl.ac.uk (Q. Liu), syazar@gtu.edu.tr (S. Yazar), f.smith@ucl.ac.uk (F. Smith).

https://doi.org/10.1016/j.taml.2022.100413

Please cite this article as: Q. Liu, S. Yazar and F. Smith, On interaction between freely moving bodies and fluid in a channel flow, Theoretical and Applied Mechanics Letters, https://doi.org/10.1016/j.taml.2022.100413

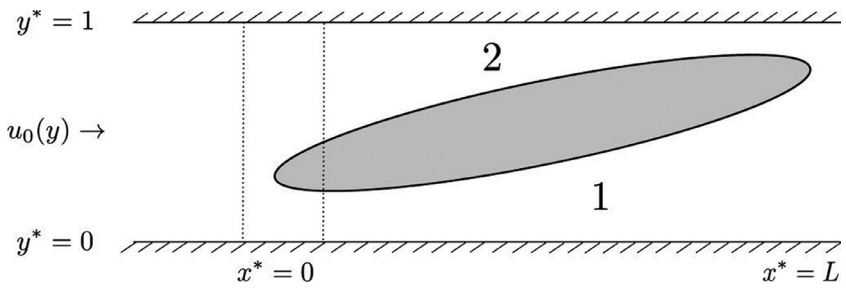

Fig. 1. One body in channel flow, indicating regions 1, 2 below and above the body respectively. Upstream influence concentrates in the dashed zone when the body length L is large. The diagram is not to scale: the horizontal (x^*) scale has been reduced in comparison with the vertical (y^*) scale.

frame fixed in the typical particle as opposed to the laboratory frame. The particles in the above study are assumed to be stacked, having identical lengths, being nearly parallel with the axial flow direction (horizontal say) and being aligned (vertically or laterally) such that their leading and trailing edges are sited at the same axial locations, namely at x values of zero and unity respectively where x denotes the scaled distance in the axial direction.

We aim to generalise the modelling in order to incorporate non-aligned bodies. That is, the bodies are taken to be stacked but with their leading and trailing edges being at different axial locations. In most applications of concern the representative Reynolds number and Froude number are very large, as in references above, and so as a very first model it seems reasonable to suppose viscous effects and gravity can be neglected. That being so we are led to the unsteady Euler equations of motion for the fluid flow and these are to be coupled with Newton's equations of motion for the bodies, yielding fluid/body interaction. The model at this stage is also to allow for the feature that the bodies of interest are slender in the sense that their typical lateral or vertical extent is significantly less than their axial or horizontal extent.

For a single particle use is made of non-dimensional variables, namely Cartesian coordinates x^* (axial), y^* (lateral), time t^*, fluid velocity vector $u^* = (u^*, v^*)$ and pressure p^*, based on the channel width vertically, the typical incident flow velocity and the density ρ_{DF} of the fluid. Assuming viscous and gravity effects are negligible as discussed in the introduction we may then work within the framework of the Euler equations,

$$\text{div } \mathbf{u}^* = 0, \ \mathrm{u}^*_{\mathrm{t}^*} + (\mathbf{u}^* \cdot \text{grad})\, \mathbf{u}^* = - \text{ grad } p^*, \tag{1}$$

as regards the fluid flow. Here 'div' and 'grad' represent divergence and gradient respectively. The boundary conditions appropriate here are kinematic boundary conditions on the moving body surfaces and tangential flow (zero normal flow) at the fixed walls, along with a match with the oncoming flow $\mathbf{u}^* = \mathbf{u}_0(y)$ with zero v^* far upstream in the channel, where p^* is taken to be zero, and, after consideration of overall conservation of mass and vorticity, the same conditions are expected to apply far downstream as well. Thus

$$\begin{aligned} &\mathbf{u}^* \rightarrow \mathbf{u}_0(y), v^* \rightarrow 0, \\ &p^* \rightarrow 0 \text{ as } x^* \rightarrow \pm\infty, \text{for } 0 < y^* < 1 \end{aligned} \tag{2}$$

There is clearly upstream influence ahead of the body and downstream influence aft of the body.

The slenderness of the body within the channel as shown in Fig. 1 now suggests scaling axial distances by the body length L ($\gg 1$). The flow then acquires an interesting structure. First, the continuity balance implies that generally the lateral flow velocity scales with L^{-1} and so the solution form

$$\begin{aligned} &(u^*, \ v^*, \ p^*) = \left(u, \ L^{-1}v, \ p\right) + \ldots, \\ &(x^*, \ y^*, \ t^*) = (Lx, \ y, \ Lt), \end{aligned} \tag{3}$$

is indicated. This long-scale form applies in the two gaps between the body surface and the wall, for $0 < x < 1$, and it leads from Eq. (1) to the slender-layer equations

$$\begin{aligned} &u_x + v_y = 0, \\ &u_t + uu_x + vu_y = -p_x(x, \ t), \\ &0 = - p_y, \end{aligned} \tag{4}$$

at leading order, where the y-momentum balance Eq. (4) leaves p depending only on x, t. Second, due to the hyperbolic nature of Eq. (4), a different solution form is found to hold near the body's leading edge $x = 0$. Here, in a region sometimes called the Euler zone [7,26],

$$\begin{aligned} &(u^*, \ v^*, \ p^*) = \mathrm{O}(1), \\ &(x^*, \ y^*, \ t^*) = (x^*, \ y, \ Lt), \end{aligned} \tag{5}$$

and so the Euler equations (1) hold in full except for the unsteady term $\mathrm{u}^*_{\mathrm{t}^*}$ which becomes negligible: the flow is thus quasi-steady. The boundary conditions on Eq. (5) include the requirement Eq. (2) as $x^* \rightarrow \infty$, tangential flow at the walls $y^* = 0, 1$ and tangential flow on the leading-edge part of the body, a part which for all the body shapes studied herein appears as a flat horizontal plate because of the slenderness of the body. As $x^* \rightarrow \infty$, on the other hand, the conditions holding can be deduced from the Bernoulli relation since the flow is quasi-steady, giving conservation of $p^* + \frac{1}{2}(u^{*2} + v^{*2})$ along streamlines. These streamlines become effectively horizontal at large negative and positive x^*, as v^* tends to zero there, and hence a match with Eq. (2) upstream and with the form Eq. (3) downstream is achieved.

In consequence the boundary conditions acting on the long-scale flow can now be written down completely. This is done here for the basic case of an incident profile $u_0(y)$=1 corresponding to uniform or so-called plug flow far upstream. The conditions are

$$\begin{aligned} &v = 0 \text{ at} \\ &y = 0, \ 1 \text{ (tangential flow on channel walls)}, \end{aligned} \tag{6a}$$

$$\begin{aligned} &v = f_{nt} + uf_{nx} \text{ at} \\ &y = f_n(x, \ t) \text{ (kinematic conditions on body surfaces)}, \end{aligned} \tag{6b}$$

$$\begin{aligned} &p + \frac{1}{2}u^2 = \frac{1}{2} \text{ at} \\ &\qquad x = 0^+ \text{ (matching with the Euler zone solution)}, \end{aligned} \tag{6c}$$

$$p = 0 \text{ at } x = 1 \text{ (the trailing} - \text{edge constraint)} . \tag{6d}$$

The condition Eq. (6c) coupled with the response Eq. (5) in the Euler zone accounts for the upstream influence mentioned earlier, while Eq. (6d) is the well-known Kutta requirement [7, 26] at the body's assumed non-blunt trailing edge. In Eq. (6b) $y = f_n(x, t)$

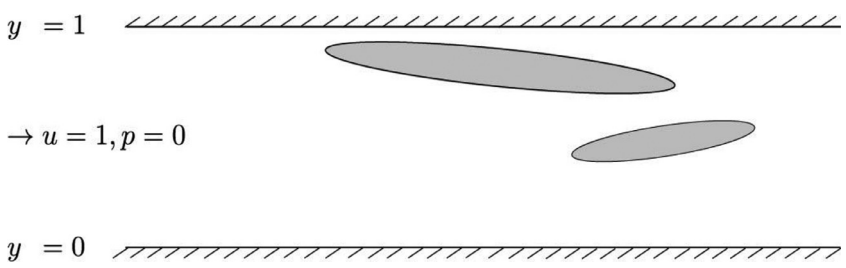

Fig. 2. Two bodies in a uniform channel flow. The diagram is not to scale; as before, the horizontal (x) scale has been reduced in comparison with the vertical (y) scale.

denotes the moving body surfaces for $n = 1, 2$. Further progress can be made by observing that the vorticity is zero to leading order in this basic case, which leads to the replacement equations

$$H_{nt} + (H_n u_n)_x = 0, \tag{7a}$$

$$u_t + uu_x = -\, p_x(x,\ t), \tag{7b}$$

where Eq. (7a) replaces Eqs. (4a), (6a) and (6b), Eq. (7b) replaces Eq. (4b, 4c) and H_n are the two gap widths, namely $H_1 = f_1(x,\ t)$ and $H_2 = 1 - f_2(x,t)$. The fluid motion is therefore governed by Eq. (7a) and (7b) subject to Eq. (6c) and (6d). Initial conditions at time zero are supposed given also.

The body motion is governed by the mass-acceleration physics of a solid body of density ρ_{DB} whose centre of mass $(x,\ y) = (C,\ h(t))$ is moving vertically, combined with a scaled rotation angle $\theta(t)$, in response to the evolving pressure field from the fluid flow. The moving body surfaces are therefore given by

$$\begin{aligned} f_1(x,\ t) &= F_1(x) + h(t) + (x - C)\,\theta(t), \\ f_2(x,\ t) &= F_2(x) + h(t) + (x - C)\,\theta(t), \end{aligned} \tag{8}$$

where $F_n(x)$ are the fixed underbody and overbody shapes, and we have at leading order the body-motion equations

$$M\frac{\mathrm{d}^2 h}{\mathrm{d}t^2} = \int (p_1(x,\ t) - p_2(x,\ t))\mathrm{d}x, \tag{9a}$$

$$I\frac{\mathrm{d}^2\theta}{\mathrm{d}t^2} = \int (x - C)\,(p_1(x,\ t) - p_2(x,\ t))\,\mathrm{d}x, \tag{9b}$$

with the prime denoting the ordinary t-derivative and $M,\ I$ denoting the scaled mass and moment of inertia of the body. Account has been taken of the small angles inherent in the current slender-body analysis as well as the fixed axial positions $x = 0,\ C,\ 1$ of the leading edge, centre of mass and trailing edge of the body respectively in the present body-based coordinate frame.

Numerical and analytical properties of the fluid/body interaction Eqs. (6c), 6d), (7a), (7b), ((8) (9a) and (9b) are investigated in Ref. [23]. There is also interest in the regime where M and I are large and comparable, which occurs if the density ratio $\rho_{DF}\ /\ \rho_{DB}$ is sufficiently small as for example with an ice particle moving through air: the density ratio in that example is about 10^{-3}. In this regime time t tends to scale like $M^{\frac{1}{2}}$ because of Eq. (9a) and (9b) and so the fluid flow becomes quasi-steady everywhere [24]. Helpful simplifications then stem from Eq. (7a) and (7b), yielding conservation of $H_n u_n$ and $p + \frac{1}{2}u^2$ in each gap.

In the next section we extend the above modelling in order to describe the fluid/body interaction when two bodies are present in a channel.

Consideration is now given to two slender bodies interacting in a channel flow as depicted in non-dimensional form in Fig. 2. The bodies are non-aligned with their leading edges at different axial stations and likewise for their trailing edges. They also overlap in the sense that the leading edge of the second body (on the right) is positioned between the leading edge and the trailing edge of the first body (the body on the left). In the laboratory frame the bodies are moving with equal horizontal components of velocity and it follows that in the current body based frame they each have zero velocity in the horizontal direction, although able to move vertically and azimuthally, to leading order.

Concerning the flow part of the fluid/body interaction, guided by the previous work as summarised in the previous section we suggest that there is a flow structure as shown in Fig. 3. This comprises five zones 1-5. In Fig. 3 the dashed lines indicate the two Euler zones, surrounding the two leading edges of the bodies, and the two trailing edges where Kutta conditions apply. The lower and upper surfaces of the first body are written $y = f_1(x,\ t)$, $y = f_2(x,\ t)$ respectively, while the lower and upper surfaces of the second body are $y = f_4(x,\ t)$, $y = f_3(x,\ t)$ respectively: we note the ordering.

The density ratio is taken to be small and hence the flow can be treated as if steady, for the sake of simplicity in the present first modelling; the flow is assumed to be forward from left to right throughout such that $u_n > 0$ for all n. So, using and extending the assumptions and notation from the previous section, we have in the successive gaps (n = 1-5) the mass balances

$$u_n H_n = d_n(\text{constants}), \tag{10}$$

where the gap widths are $H_1 = f_1, H_2 = 1 - f_2, H_3 = f_1 - f_3, H_4 = f_4, H_5 = 1 - f_3$. Similarly the usual Bernoulli quantity is conserved throughout the zones 1-5 because of the known properties of the Euler regions and hence

$$p_n + \frac{1}{2}\frac{d_n^2}{H_n^2} = \frac{1}{2}, \tag{11}$$

again holding for n = 1-5. There are expected to be jumps in pressure p and velocity u across the Euler regions in general but the quantities in Eq . (11) remain conserved across those regions.

Next, the total mass fluxes must be taken into account. These require the following relations to hold,

$$d_1 + d_2 = 1,\ d_3 + d_4 = d_1,\ d_2 + d_3 = d_5. \tag{12}$$

(From the above relations we see that the required balances $d_4 + d_5 = d_1 + d_2 = 1$ also hold.) Also the Kutta conditions at the two trailing edges $x = b,\ x = c$ are that the pressures there are equal, leading from Eq. (11) to the equations

$$\frac{d_2^2}{H_2(b,t)^2} = \frac{d_3^2}{H_3(b,t)^2}, \tag{13}$$

and

$$\frac{d_4^2}{H_4(c,t)^2} = \frac{d_5^2}{H_5(c,t)^2}, \tag{14}$$

in turn. The equality of the values in Eq. (13) with the value $\frac{d_5^2}{H_5(b,t)^2}$ implied by zone 5 is found to be assured, i.e. it is guaranted by the displayed equations above.

Thus there are five equations Eqs. (12), (13) and (14) for the five unknowns $d_1 - d_5$. The balances Eqs. (13) and (14) can now be

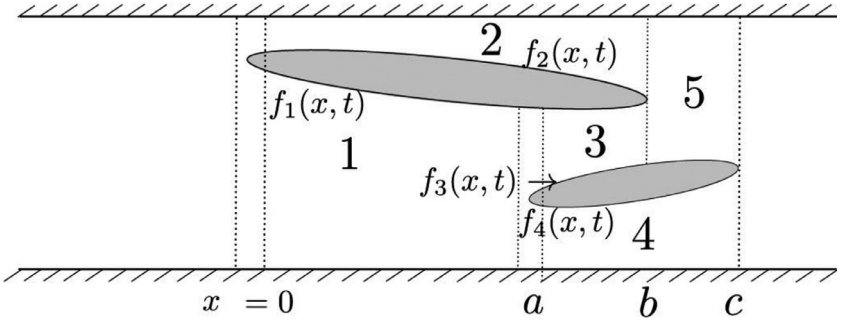

Fig. 3. The interactive structure for two bodies, showing zones 1-5.

simplified to give

$$\frac{d_2}{H_2(b,t)} = \frac{d_3}{H_3(b,t)}, \quad \frac{d_4}{H_4(c,t)} = \frac{d_5}{H_5(c,t)}, \tag{15}$$

since all the velocities u_n are positive. Hence the solutions are found to be

$$d_1 = 1 - \frac{H_2(b,t)H_5(c,t)}{H_5(b,t)}, \tag{16a}$$

$$d_2 = \frac{H_2(b,t)H_5(c,t)}{H_5(b,t)}, \tag{16b}$$

$$d_3 = \frac{H_3(b,t)H_5(c,t)}{H_5(b,t)}, \tag{16c}$$

$$d_4 = H_4(c,t), \tag{16d}$$

$$d_5 = H_5(c,t). \tag{16e}$$

These are to be used in conjunction with the body-movement properties described below. It is notable meanwhile that a non-overlapping scenario would involve zero feedback between the two bodies because of the Kutta condition and the ensuing lack of a wake in the present quasi-steady flow model for small density ratios.

Concerning the body motions, the two bodies have to move by virtue of the mass-acceleration effects. Thus

$$M_1 \frac{\mathrm{d}^2 h_1}{\mathrm{d}t^2} = \int_0^a (p_2 - p_1)\mathrm{d}x + \int_a^b (p_2 - p_3)\mathrm{d}x, \tag{17a}$$

$$I_1 \frac{\mathrm{d}^2 \theta_1}{\mathrm{d}t^2} = \int_0^a (x - \alpha_1)(p_2 - p_1)\mathrm{d}x + \int_a^b (x - \alpha_1)(p_2 - p_3)\mathrm{d}x, \tag{17b}$$

for the first body and

$$M_2 \frac{\mathrm{d}^2 h_2}{\mathrm{d}t^2} = \int_a^b (p_3 - p_4)\mathrm{d}x + \int_b^c (p_5 - p_4)\mathrm{d}x, \tag{18a}$$

$$I_2 \frac{\mathrm{d}^2 \theta_2}{\mathrm{d}t^2} = \int_a^b (x - \alpha_2)(p_3 - p_4)\mathrm{d}x + \int_b^c (x - \alpha_2)(p_5 - p_4)\mathrm{d}x, \tag{18b}$$

for the second body. The right-hand sides in Eqs. (17) and (18) depend on the pressure differences to be calculated from the fluid flow. We also need to relate h_1, θ_1, h_2, θ_2 to the gap widths $H_1 - H_5$ and to the prescribed shapes of the body surfaces.

The properties resulting from the interactive equations of the fluid flow in Eqs. (11)-(16) and the bodies' motions in Eqs. (17) and (18) are invetstigated in the following section.

Here for the sake of numerical and analytical study we would like to consider concrete examples of the previous model configurations. What we are particularly interested in is investigating how to make particles remain between the parallel channel walls for as long as possible without any impacting on each other or on the walls. Our current study stops when one of the particles collides with the wall, either the top or the bottom wall, or when there is a particle-particle impact. It is necessary now to address specific examples.

In detail, the equations for the unknown moving body surfaces are now taken to be as follows,

$$f_1(x,t) = F_1^-(x) + h_1(t) + \left(x - \frac{1}{2}\right)\theta_1(t), \tag{19}$$

$$f_2(x,t) = F_1^+(x) + h_1(t) + \left(x - \frac{1}{2}\right)\theta_1(t) \tag{20}$$

$$f_3(x,t) = F_2^+(x) + h_2(t) + \left[(x - 0.8) - \frac{1}{4}\right]\theta_2(t), \tag{21}$$

$$f_4(x,t) = F_2^-(x) + h_2(t) + \left[(x - 0.8) - \frac{1}{4}\right]\theta_2(t), \tag{22}$$

where Eqs. (19) and (20) represent the lower and upper shape functions for particle 1 respectively, while Eqs. (21) and (22) represent the upper and lower shape functions for particle 2 respectively.

In addition, particle 1 has its leading edge at $x = 0$ and its trailing edge at $x = 1$, thus having unit length, whereas particle 2 has length $\frac{1}{2}$ with its leading and trailing edges being at $x = 0.8$ and $x = 1.3$ in turn. The respective centres of mass are located at the halfway positions, namely $x = 0.5$ and $x = 1.05$. We also define our particles to be elliptically shaped. Thus here we define the particle shape functions as

$$F_1^+(x) = \alpha_1 + x^{\frac{1}{2}}(1 - x)^{\frac{1}{2}}\beta_1, \tag{23}$$

$$F_1^-(x) = \alpha_1 - x^{\frac{1}{2}}(1 - x)^{\frac{1}{2}}\beta_1, \tag{24}$$

$$F_2^+(x) = \alpha_2 + (x - 0.8)^{\frac{1}{2}}(1.3 - x)^{\frac{1}{2}}\beta_2, \tag{25}$$

$$F_2^-(x) = \alpha_2 - (x - 0.8)^{\frac{1}{2}}(1.3 - x)^{\frac{1}{2}}\beta_2, \tag{26}$$

with positive thickness constants β_1, β_2 and leading edge heights α_1, α_2. Typical studies described here are for $(\alpha_1, \alpha_2, \beta_1, \beta_2)$ equal to (0, 0, 0.1, 0.05) and initial conditions $(h_1, \frac{\mathrm{d}h_1}{\mathrm{d}t}, h_2, \frac{\mathrm{d}h_2}{\mathrm{d}t})(0)$ equal to (0.7, 0, 0.4, 0). During the course of the study, we tested many different values of initial angles and angular velocities but among

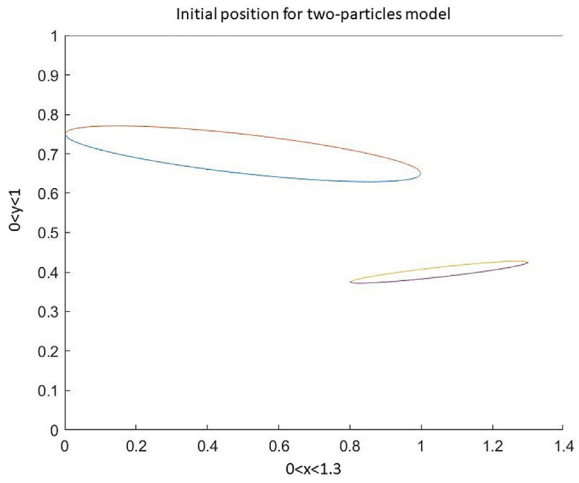

Fig. 4. Time $t = 0$

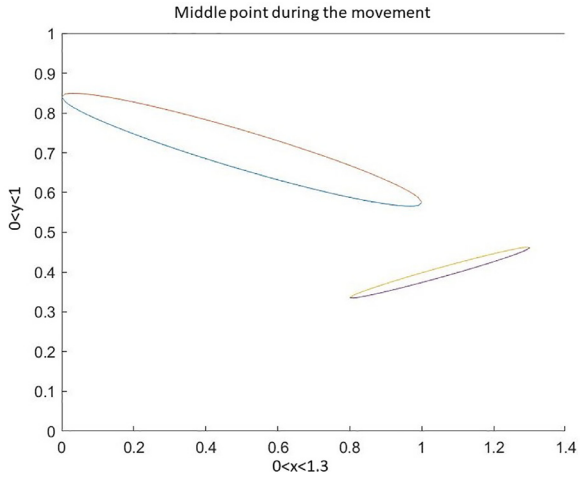

Fig. 5. Time $t = 0.17$

them interesting values were found to be $\theta_1(0)$= -0.1, $\theta_2(0) = 0.1$ with $\frac{d\theta_1}{dt} = -1$ and $\frac{d\theta_2}{dt} = 1$. We also set the moment of inertia of particle 1 to be $I_1 = 0.25 \times M_1$ and particle 2 to be $I_2 = 0.1 \times M_2$.

In the following figures which show numerical solutions we plot three examples (1)-(3) with different mass values as described below.

(1) We set $M_1 = 1$ and $M_2 = 1$

Figure 4 is the initial starting point of the whole system. Figure 5 shows in a sense the middle stage of the whole movement. Figure 6 is at the collision time where particle 1 impacts upon the upper wall. As we can see from the graph, the particle 1 moves upwards and rotates clockwise. The height of the centre of mass for particle 2 remains almost constant and its motion is almost only a rotation, slightly upward and anticlockwise.

In order to make a clear contrast with this group, we next took two extreme values and tested them.

(2) We set $M_1 = 16$ and $M_2 = 1$ and keep other values the same as in example (1).

Here Fig. 7 is the initial starting point of the whole system, Fig. 8 is the middle stage of the evolution and Fig. 9 is essentially at the collision time. Despite the increased mass of particle 1 in example (2) we have almost the same motion as in example (1) except that the collision happens somewhat later than in example (1).

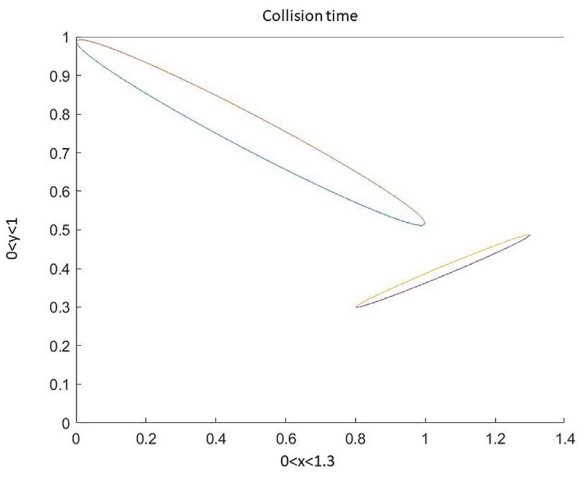

Fig. 6. Time $t = 0.33$

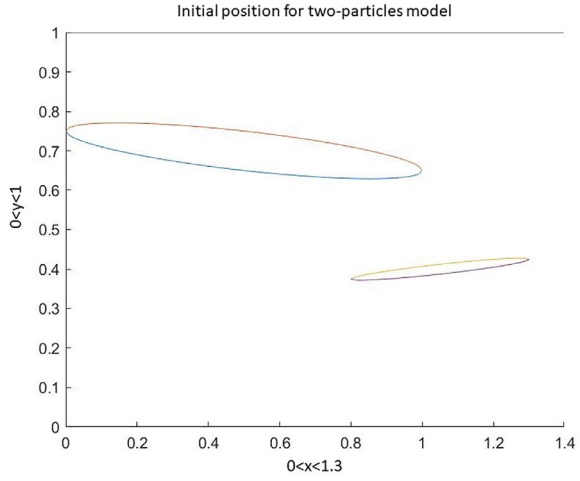

Fig. 7. Time $t = 0$

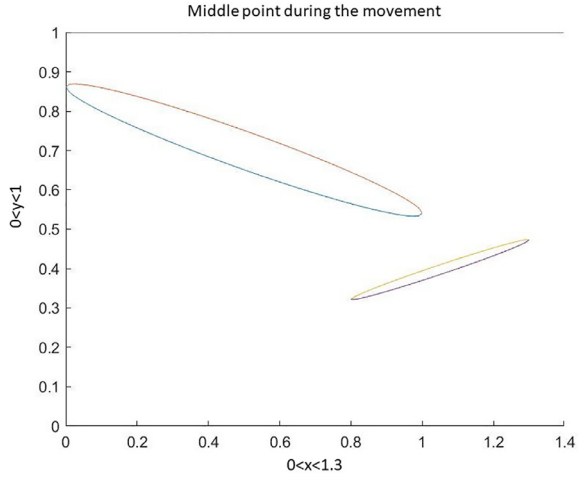

Fig. 8. Time $t = 0.23$

(3) We set $M_1 = 1$ and $M_2 = 16$ and keep other values same as for example (1).

Again Fig. 10 is the initial starting point of the whole system. Figure 11 is the middle stage of the whole movement. Figure 12 is at the collision time. We have almost the same motion as in example (1). From the graphs we notice that there is a tiny difference

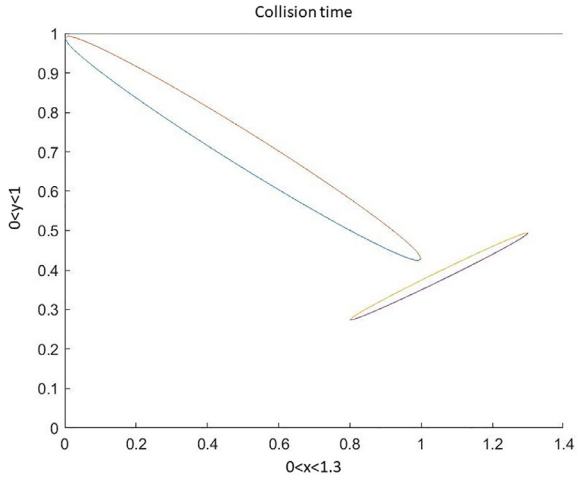

FIG. 9. time $t = 0.46$

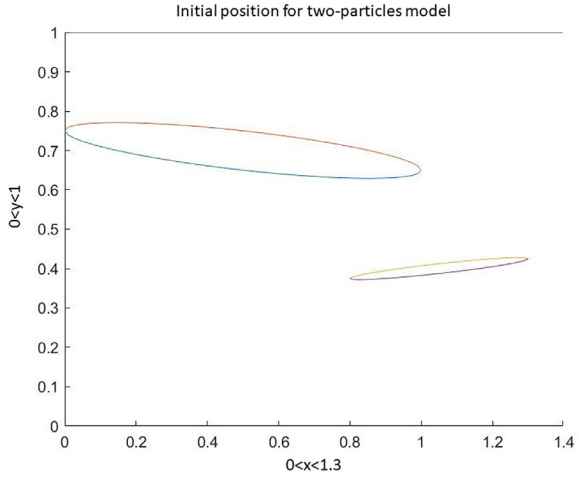

FIG. 10. time $t = 0$

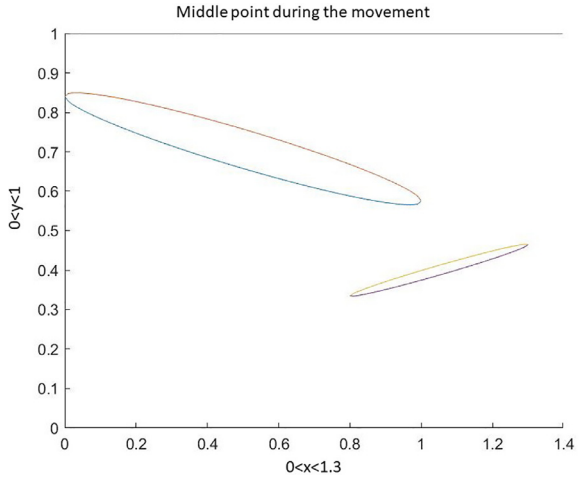

FIG. 11. time $t = 0.17$

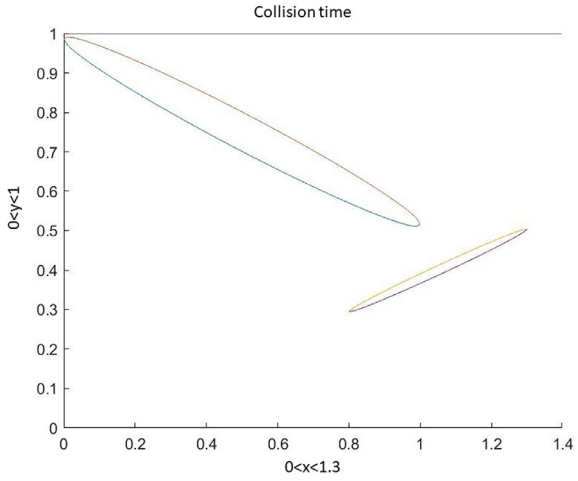

Fig. 12. Time $t = 0.33$

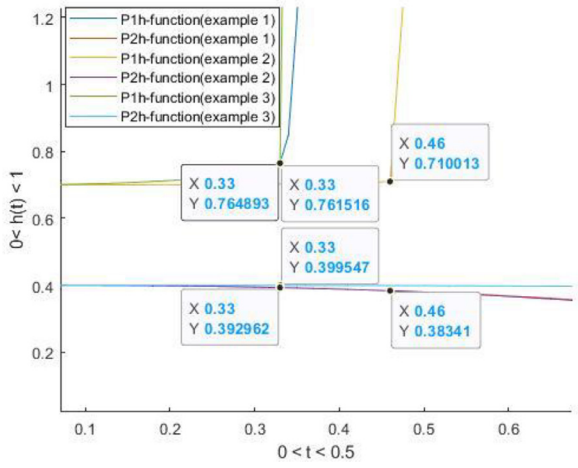

Fig. 13. Height functions for the two-particle model in three examples.

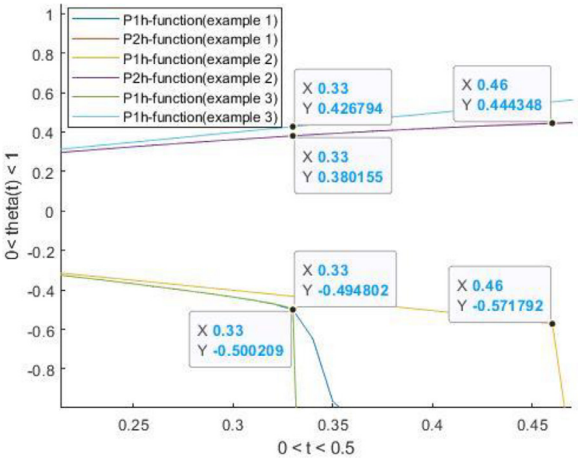

Fig. 14. θ functions for the two-particle model in three examples.

between examples (1) and (3) (and likewise between examples (1) and (2)). This might well be caused by the different mass of particle 2. With larger mass and moment of inertia, particle 2 is harder to stop in a sense; its motion is virtually ballistic. In particular the displacement of particle 2 in example (3) is larger than that in example (1).

The height and theta functions for these three examples are presented in Figs. 13 and 14.

Figure 13 gives a graph showing the height trajectories of each case. The top three lines represent the trajectories for particle 1 in these three examples and the bottom three lines represent the trajectories for particle 2. From the sudden change of the height functions for particle 1 we can read that the collision happened

between particle 1 and the top wall. That is, the fluid gap there closed at a finite time, after which the results are unphysical. Similarly, we plot the theta functions for particles in these three cases in Fig. 14.

Figure 14 presents the θ trajectories of each case. In contrast to the height trajectory, the bottom three lines represent the θ trajectories for particle 1 and the top three lines represent the θ trajectories for particle 2. Once again the collision time is indicated by the rapid turning point in the results.

Analysis provides some insight here. When M_1 and I_1 are large the suggestion is that, to leading order, the equations for particle 1 become simply

$$M_1 \frac{\mathrm{d}^2 h_1}{\mathrm{d}t^2} = 0, \; I_1 \frac{\mathrm{d}^2 \theta_1}{\mathrm{d}t^2} = 0, \tag{27}$$

for times t of order unity. Hence

$$h_1 = h_1(0), \; \theta_1 = \theta_1(0) + \theta_1'(0)t, \tag{28}$$

for all such t. In our model we can regard $M = 16$ as large enough to use the above analysis. Thus for the case of $M_1 = 16$ and $M_2 = 1$, the asymptotic analysis shows that particle 1 is free to rotate about its centre of mass $x = \frac{1}{2}$ at a constant rotation rate (constant angular velocity) which is -1, from the initial conditions. In effect the centre of mass of particle 1 stays still. Hence the leading edge rises uniformly and the trailing edge falls uniformly. (Particle 1 is in essence independent of particle 2 in this extreme.) However, particle 1 is long compared with particle 2 and so the leading and trailing edges of particle 1 appear to be displaced by large amounts compared with the movement of the smaller particle 2. For the $M_1 = 1$ and $M_2 = 16$ case, similarly, the leading and trailing edges of particle 2 move up or down uniformly and its centre of mass effectively stays still, in line with the asymptotic behaviour

$$h_2(t) = h_2(0), \; \theta_2(t) = \theta_2(0) + \theta_2'(0)t, \tag{29}$$

for t of order unity. However, particle 2 is the shorter particle and so its displacement appears smaller in the results.

The analytical trends Eqs. (28) and (29) appear to agree with those of the numerical solutions in Figs. 4-14. The analysis behind forms Eqs. (28) and (29) also suggests repeating the numerical study of case (3) but with the initial rotation $\theta_2'(0)$ increased to 4 and the initial vertical distances between the centres of mass decreased, in which case particle 2 might be expected to collide with particle 1 before any other collision can occur. Thus an additional example (4) is examined next.

(4) We set $\theta_2'(0) = 4$ and $h_1(0) = 0.5$ and keep other values the same as for example (3).

The result is given in Fig. 15 and 16.

The finding in case (4) is that, whereas in the earlier cases the gap between the two particles is too large to let them collide with each other (before hitting a wall), now a collision can occur between the particles due to the change of initial height of particle 1 from 0.7 to 0.5 and the enlarged initial rotation of particle 2. A consequent body-to-body collision time of about $t = 0.14$ is seen to be encountered.

It is felt that the examples (1)-(4) as described above indicate the two types of impact phenomena likely to be present in the two-body fluid/body interaction problem in a channel. The types are body-wall and body-body impacts. The examples also suggest that further analysis on parametric influences could be especially fruitful. It is to be expected that many other specific cases lead potentially to the occurrence of the two types of impact above.

The present work points immediately to a number of useful follow-up studies and also to addressing certain difficult issues of combined fluid and solid mechanics.

One natural follow-on is to extend the understanding to the case of many bodies being present in the channel. This has only been done in the aligned scenario of Ref. [7]. In the more general non-aligned setting we can begin by creating a model for three free particles. Extending the model of the previous sections to three bodies leads to the interactive solution structure displayed in Fig. 17. The figure gives one example of how the three leading edge positions and the three trailing edge positions of the bodies can overlap but in all examples there must be three short-scale Euler zones and three Kutta conditions to apply, a feature which guides the subsequent working. In this example eight separate long-scale regions are present as shown in the figure.

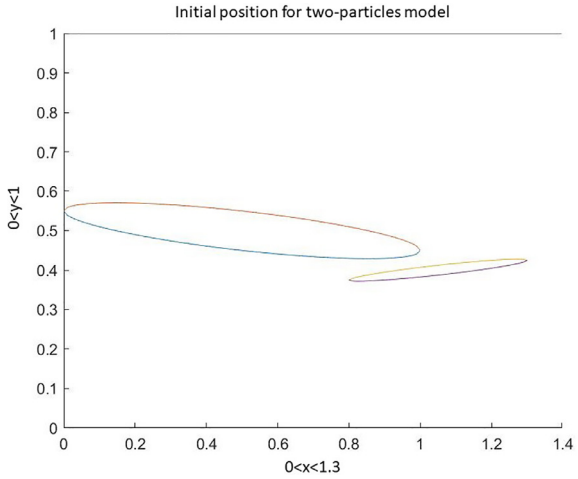

Fig. 15. Time t = 0

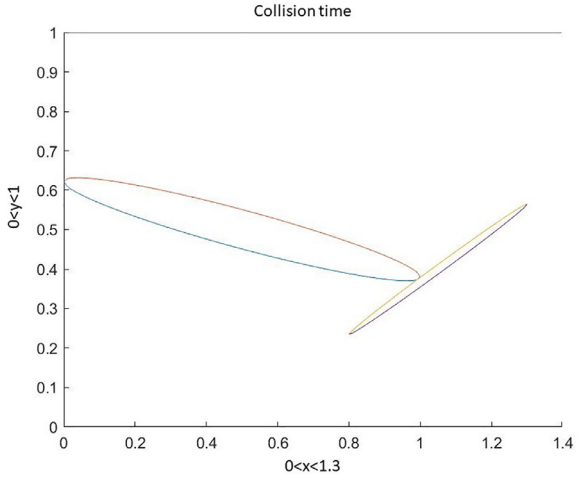

Fig. 16. Time t = 0.14

The governing equations in the eight regions are analogous, thus yielding

$$u_n H_n = d_n \text{ (constants)}, \tag{30}$$

$$p_n + \frac{1}{2}\frac{d_n^2}{H_n^2} = \frac{1}{2}, \tag{31}$$

for n = 1-8 where the gap widths $H_n(x,t)$ are defined by differences between adjacent body positions or between a body position and the adjacent wall of the channel. Because of the number of leading and trailing edges the total mass fluxes then require the six relations

$$\begin{aligned} &d_1 + d_2 = 1, d_3 + d_7 = d_1, \\ &d_4 + d_5 = d_2, \; d_3 + d_4 = d_6, \\ &d_5 + d_6 = d_8, \; d_7 + d_8 = 1, \end{aligned} \tag{32}$$

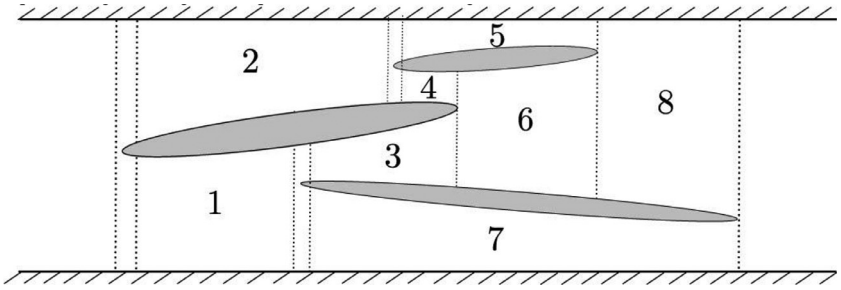

Fig. 17. Sketch of the three-body problem and its solution structure.

to hold. Notably the final relation Eq. (32) is linearly dependent on the other relations. Further the Kutta conditions at the three trailing edges, say $x = b,\ x = c,\ x = d$ point to the equations

$$\frac{d_3^2}{H_3(b,t)^2} = \frac{d_4^2}{H_4(b,t)^2}, \tag{33}$$

$$\frac{d_5^2}{H_5(c,t)^2} = \frac{d_6^2}{H_6(c,t)^2}, \tag{34}$$

$$\frac{d_7^2}{H_7(c,t)^2} = \frac{d_8^2}{H_8(c,t)^2} \tag{35}$$

in turn. The eight equations Eqs. (32)-(35) can then be solved for the eight unknowns

d_1-d_8 in order to provide the pressure distributions p_n. The latter act as forcing effects in the body-motion balances which are analogous with Eqs. (17a), (17b), (18a) and (18b) but extended for three bodies, i.e. involving unknown functions of time $(h_1,\ \theta_1),\ (h_2,\ \theta_2)$ and $(h_3,\ \theta_3)$. The solution responses remain to be pursued.

Challenging issues are also involved in tackling several extra aspects of fluid/body interactions relevant to the current area. These include in particular: different horizontal speeds of the bodies in the laboratory frame, causing slip in the body based frame and hence time-dependent overlaps; rebounds after clashes (in particular a post-collision two-particle model will be investigated in future research); the effects of viscosity, three-dimensionality and surface flexibility; comparison of the predictions from unsteady and quasi-steady flow; the full influence of body shapes and wall shapes. Just as there are many parameter regimes to study, there are in addition many interesting shapes to consider. These extra issues should enable the connection with practical applications to be made firmer.

The two-dimensional fluid/body interaction arising when fast-moving bodies, or particles of finite size, are free to move within the fluid surrounding them has been studied. New modelling and results on the behaviour of two interacting bodies inside a channel flow have been described for an assumed inviscid fluid. The extension to more bodies has also been discussed with a view to treating arrays of non-aligned bodies in a rational manner. For the case of many bodies the role of overlap as described is notable. Thus if there are groups of bodies separated by vertical gaps, i.e. not overlapping, then the feedback between the groups is negligible even if the groups are nearby each other; the absence of significant flow separation and hence the absence of significant wakes for the present slender bodies is a substantial factor here. For the case of two overlapping bodies it has been found specifically that the initial conditions and the relative body masses and moments of inertia exert considerable influence not only on the occurrence of body-body impacts as distinct from wall-body impacts but also on the corresponding impact times. (Both the wall-body and the body-body impacts in the present context of quasi-steady fluid flow can be described locally by analyses akin to those applied in recent work [25] within the context of a boundary layer.)

The modelled interaction between fluid flow dynamics and the free movement of bodies holds over a wide range of scales, from macro- to nano-scales. Here the potential relevance to industry, aerodynamics, biomedicine and the environment seems positive. In terms of understanding the mechanics and the physical aspects, it is felt that there is far more still to be explored (on three-dimensional effects, on many-particle interactions, on nonlinear and conventional instability effects for example) than has been done to date in the area. Continuing studies along the current lines are concerned with skimming, with the growth or erosion of ice on a substrate, and with tackling three-dimensional interactions as well as with attempting to accommodate many bodies as described in the previous section. The combination of physical modelling, analysis and allied computation, whether small-scale or large-scale, appears to have been beneficial in this work.

Declaration of Competing Interest

The authors declare that they have no known competing financial interests or personal relationships that could have appeared to influence the work reported in this paper.

Acknowledgment

The authors are grateful to a referee for helpful comments as well as for encouraging remarks.

References

[1] R.W. Gent, N.P. Dart, J.T. Cansdale, Aircraft icing, Philos. Trans. R. Soc. Lond. Ser. A 358 (2000) 2873–2911.
[2] R Purvis, F T Smith, Mulholland Aston, Improving aircraft safety in icing conditions, Chapter in UK Success Stories in Industrial Mathematics, Springer, 2017 Tant.
[3] E. Norde, Eulerian method for ice crystal icing in turbofan engines, University of Twente, 2017 PhD Thesis.
[4] T.W. Secomb, R. Skalak, N. Ozkaya, et al., Flow of axisymmetric red ¨blood cells in narrow capillaries, J. Fluid Mech. 163 (1986) 405–423.
[5] Y. Iguchi, K. Kimura, A case of brain embolism during catheter embolisation of head arteriovenous malformation. what is the mechanism of stroke? J. Neurol. Neurosurg. Psychiatry 78 (2007) 81 –81.
[6] M. Andrew, M. David, G. deVeber, et al., Arterial thromboembolic complications in paediatric patients, Thromb. Haemostasis 78 (1997) 715–725.
[7] F.T. Smith, A.S. Ellis, On interaction between falling bodies and the surrounding fluid, Mathematika 56 (2010) 140–168.
[8] F.T. Smith, P.L. Wilson, Fluid–body interactions: clashing, skimming, bouncing, Philos. Trans. R. Soc., A 369 (2011) 3007–3024.
[9] S. Balta, F. T. Smith, Fluid flow lifting a body from a solid surface, Proc. R. Soc. A 474 (2018) 2219.
[10] K. Liu, F.T. Smith, Collisions, rebounds and skimming, Philosophical Transactions of the Royal Society A: Mathematical, Phys. Eng. Sci. 372 (2014) 20130351.
[11] E.M. Jolley, R.A. Palmer, F.T. Smith, Particle movement in a boundary layer, J. Eng. Math. 128 (2021) 1–19.
[12] K. Liu, F.T. Smith, A smoothly curved body skimming on shallow water, 185 J. Eng. Math. 128 (2021) 1–15.

[13] A. Kudrolli, D. Scheff, B. Allen, Critical shear rate and torque stability condition for a particle resting on a surface in a fluid flow, J. Fluid Mech. 808 (2016) 397–409.
[14] M.S. Akoz, M.S. Kirkgoz, Numerical and experimental analyses of the flow around a horizontal wall-mounted circular cylinder, Trans. Can. Soc. Mech. Eng. 33 (2009) 189–215.
[15] P. Diplas, C.L. Dancey, A.O. Celik, et al., The role of impulse on the initiation of particle movement under turbulent flow conditions, Science 322 (2008) 717–720.
[16] R.A. Palmer, F.T. Smith, A body in nonlinear near-wall shear flow: numerical results for a flat plate, J. Fluid Mech. 915 (2021).
[17] R.A. Palmer, F.T. Smith, A body in nonlinear near-wall shear flow: impacts, analysis and comparisons, J. Fluid Mech. 904 (2020) A32.
[18] R. Palmer, F. Smith, When a small thin two-dimensional body enters a viscous wall layer, Eur. J. Appl. Math. 31 (2020) 1002–1028.
[19] F.T. Smith, Free motion of a body in a boundary layer or channel flow, J. Fluid Mech. 813 (2017) 279–300.
[20] R. Palmer, I. Roberts, R. Moser, et al., Non-spherical particle trajectory modelling for ice crystal conditions, SAE Technical Paper, 2019 Technical Report.
[21] A S Ellis, Modelling chute delivery of grains in a food-sorting process, University College London, 2008 PhD thesis.
[22] F T Smith, S Balta, K Liu, et al., On dynamic interactions between body motion and fluid motion, Chapter in Mathematics Applied to Engineering, Modelling, and Social Issues, Springer, 2019 Mordenson.
[23] S. Balta, On fluid-body and fluid-network interactions, University College London, 2017 PhD thesis.
[24] Q. Liu, Interactions, impacts and rebounds of fluid and body motions in channels. PhD thesis, University College London. 2023-24
[25] E.M. Jolley, F.T. Smith, A heavy body translating in a boundary layer: 'crash', 'fly away' and 'bouncing' responses, J. Fluid Mech. 936 (2022) A37, doi:10.1017/jfm.2022.93.
[26] H. Schlichting, K. Gersten, Boundary-Layer Theory, Springer, 2017.